

# Flow behaviour of granular materials: modelling wall adhesion and its impact on grain segregation

Neel Raghav, S. Joseph Antony\*, and Ali Hassanpour

School of Chemical and Process Engineering, University of Leeds, LS2 9JT, UK

**Abstract** Granular assemblies, composed of large collections of discrete, macroscopic particles, exhibit complex and often unpredictable behaviours during flow. For instance, discharge of granular materials from a hopper can result in particles segregating by size, and the role of wall adhesion in this process remains underexplored. This study uses Discrete Element Modelling (DEM) to examine how wall adhesion affects particle segregation and mound formation on discharge. A bin-based method from [4] is employed to assess segregation under gravity in mass flow and funnel flow geometries. Segregation in both geometries is primarily driven by percolation during loading. In mass flow, wall adhesion primarily affects finer particles at lower regions, influencing their initial flow patterns, while its impact on larger particles increases with height. In funnel flow, adhesion influences larger particles throughout the system, with strong adhesion values ( $>0.025 \text{ J/m}^2$ ) impeding finer particle flow at higher levels, ultimately reversing initial segregation trends. This results in layered segregation across different flow phases, producing distinct stratified layers in the discharge mound.

## 1 Introduction

Granular assemblies are large collections of discrete particles and exhibit complex flow behaviour [1]. In the UK, around 75% of chemical industry processes involve particulate solids [2], contributing significantly to economic value. Here, manufacturing adds £224 billion GVA (2023), employs 2.6 million people, and accounts for 49% of exports [3]. As of 2021, around £34 billion is invested annually in the manufacturing sector [3].

Granular assemblies are made of particles with varying size, density, and shape [4,5]. During handling and motion, they tend to segregate, affecting product homogeneity [5]. DEM simulations have been used to analyse this by dividing the discharge mound into bins [4]. Segregation is mainly driven by percolation—fine particles fall through shear-induced voids while larger ones rise [5,6]. Trajectory segregation also occurs due to friction-induced velocity differences [6]. Information is currently lacking on the effects of wall adhesion on the segregation characteristics of granular flows in hoppers.

Discrete Element Modelling (DEM), a dynamic 3D simulation technique [7,8], is used here to study grain segregation in hopper flow. Extending prior DPIV-based studies [1], this work models  $30^\circ$  (uniform flow) and  $60^\circ$  (funnel flow) hopper geometries. DEM simulations assess how varying wall adhesion affects segregation.

## 2 Methodology

### 2.1 Particle and geometry properties

The simulations utilised the properties of granular assembly and hopper geometries defined in [1], featuring wet granulated corn starch within a Perspex conical hopper. The physical and mechanical properties of both the particles and the hopper are provided in Table 1.

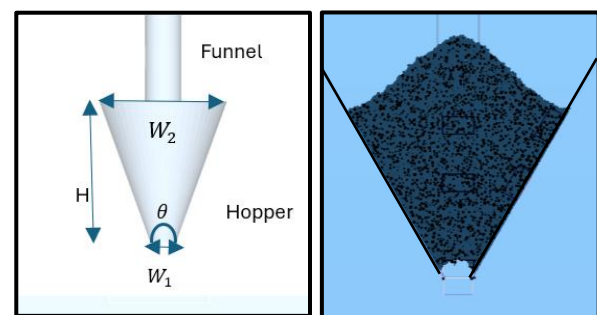
Table 1: Physical, mechanical, and interaction properties of corn starch grains and contacting Perspex walls

Parameter (Units)	Corn starch particles	Reference	Perspex sheet	Reference
Seed Poisson's Ratio	0.35	[4]	0.25	[4]
True Density ( $\text{g/cm}^3$ )	$1.5014 \pm 0.0001$	[1]	1.180	[4]
Young's Modulus (Pa)	$1 \times 10^8$	[9]	$2.5 \times 10^9$	[4]
Static angle of repose ( $^\circ$ )	$(38.12)^\circ \pm 0.41$	[1]	-	-
Coefficient of Restitution	0.6	[4]	0.4	[4]
Coefficient of static friction	0.3	[4]	0.5	[4]
Coefficient of rolling friction	0.2	[4]	0.1	[4]

The grains were characterised, resulting in a mean diameter of  $650\mu\text{m}$ , with a diameter range of  $300\text{--}1000\mu\text{m}$  and an angle of repose of  $(38.12)^\circ \pm 0.41$  [1].

### 2.2 Geometry design

The hopper geometry used is shown in Figure 1, and a filled hopper slice is shown in Figure 2. Table 2 shows the DEM input parameters for both geometries.



Figures 1 [Left] and 2 [Right]:  
 Figure 1 is a schematic diagram of the  $30^\circ$  ( $\theta$ ) hopper geometry created.  
 Figure 2 shows a snapshot of particle flow through the  $60^\circ$  hopper in the DEM simulation.

\*Correspondence: S.J.Antony@leeds.ac.uk

Table 2: Input parameters for the design of the geometries

Parameter	30° Hopper	60° Hopper
H (m)	0.08	0.08
$W_1$ (m)	0.0105	0.0105
$W_2$ (m)	0.0534	0.1029
$\theta$ (°)	30°	60°

The angle  $\theta$  represents the hopper's opening angle. The orifice width ( $W_1$ ) was set at 10.5 times the mean particle diameter ( $d$ ) to minimise arching effects and ensure continuous flow [2]. The top width ( $W_2$ ) was determined as a function of the opening angle and orifice width. The hopper's vertical height (H) from the orifice was 8 cm ( $80d$ ). Particles were generated into a virtual funnel above the hopper. This meant a fixed number of particles were generated within the funnel at a defined time [8], and the process continued until the required height of particles was filled. A simulation box was placed below to analyse discharge segregation.

### 2.3 Calibration for inter-particle cohesion

Within the simulation, to reduce the number of particles and ease computational requirements, the particles were scaled to a mean diameter of  $1000\mu\text{m}$ , with the diameter range of  $500\mu\text{m} - 1500\mu\text{m}$  (0.5-1.5 mean diameter) across a normal size distribution. All other variables, such as particle stiffness and density, were not scaled. The new particles were then fine-tuned to match the angle of repose from the literature in [1],  $(38.12)^\circ \pm 0.41$ .

Inter-particle cohesion was modelled in Altair EDEM using the Hertz-Mindlin with JKR contact model, requiring a surface energy input. To calibrate this for wet granulated corn starch, the surface energy value was tuned based on literature [4]. An initial value of  $0.045\text{ J/m}^2$  for starch [9] was assigned in DEM. Particles were generated and loaded into a closed hopper, which was then opened to discharge them into a simulation box. Once settled, the mound's angle of repose was measured and compared to the actual value [1]. The surface energy was iteratively adjusted as  $0.015\text{ J/m}^2$ ,  $0.0125\text{ J/m}^2$  and  $0.01\text{ J/m}^2$ , producing an angle of repose of  $43.8^\circ$ ,  $41.1^\circ$ , and  $38.6^\circ$  respectively. Hence,  $0.01\text{ J/m}^2$  was selected for the inter-particle adhesion studies as this closely matched the experimental reference value [1].

### 2.4 Simulating particle segregation

Particles were loaded into the hopper along the central axis via a funnel, following the approach in [1]. This was done using randomly generated particles, ensuring no segregation occurred before loading. Segregation on loading was minimised by loading the particles across multiple layers; 15 layers for the 30° hopper and 31 layers for the 60° hopper. This is a method of industrial filling type aimed at minimising segregation [10], though details are yet scarce. Each layer in the 30° hopper had 3,000 particles, totalling 45,000 particles. In the 60° hopper, the first five layers had 3,000 particles each, while subsequent layers contained 5,000 particles, totalling 145,000 particles. This helped isolate the impact of adhesion in different regions of the geometry.

Wall adhesion was varied across  $0\text{ J/m}^2$  (non-adhesive),  $0.01\text{ J/m}^2$ ,  $0.025\text{ J/m}^2$ ,  $0.035\text{ J/m}^2$ , and  $0.045\text{ J/m}^2$  to assess its effect on segregation. Simulations were conducted under a fixed gravitational acceleration of  $9.81\text{ m/s}^2$ . Interparticle cohesion remained constant. Particles were filled to the top of the geometry (Fig. 2) to ensure a significant number of particles came into contact with the wall.

### 2.5 Data extraction – Segregation

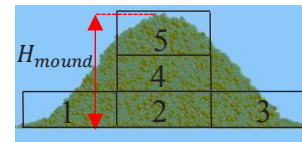


Figure 3: The bins created to evaluate segregation on discharge for the 30° geometry

The methodology from [4] was used to analyse segregation by dividing the discharge mound into distinct virtual bins and studying the distribution of large and small particles within each bin. Figure 3 illustrates the bin configuration. The bins were studied in a fixed plane with a thickness of 6 times the average diameter of particles (sliced along the central axis), as due to the assumed axi-symmetric nature of the hopper and the discharged mound. Each bin had the same width, but the height of the bin was judged to be  $\frac{H_{mound}}{3}$ . Bin 2 represents particles that exited the hopper during initial discharge, while Bin 4 captures particles discharged during bulk flow. Bins 1, 3, and 5 track the final particles leaving the hopper. The largest 20% of particles ( $d = 0.0013\text{m}$  to  $d = 0.0015\text{m}$ ) and the smallest 20% ( $d = 0.0005\text{m}$  to  $d = 0.0007\text{m}$ ) were extracted, and their distribution was analysed by calculating the ratio of the largest to the smallest particles (referred to as ratio of big to small particles). This was done to ensure that the results maintained proportionality, irrespective of the number of particles in the bins.

## 3 Results and discussion

### 3.1 Analysis for the mass flow (30°) geometry

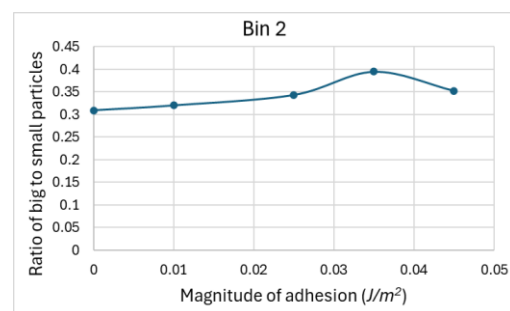


Figure 4: Ratio in bin 2 for 30° geometry

The observed trend indicates that the bins corresponding to the initial particle outflow and bulk flow—bins 2 and 4 (Figs. 4 and 5)—contain a higher proportion of smaller particles, with large-to-small particle ratios of less than 0.4. In contrast, Figs. 6 and 7 show large-to-small

particle ratios ranging from 1.2 to 1.8 across all adhesive wall functions. This demonstrates significant percolation-driven segregation.

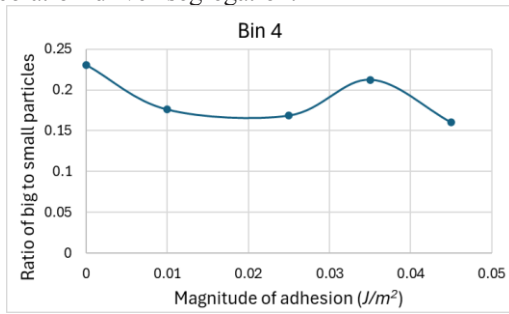


Figure 5: Ratio in bin 4 for 30° geometry

Figures 4 and 5 show that as adhesion increases, the proportion of larger particles in Bin 2 rises, while the opposite trend is observed in Bin 4. This occurs because Bin 2 shows the first phase of flow, where the narrow outlet geometry results in more particle-wall contact. Here, smaller particles experience greater flow impedance due to adhesion, altering their trajectory and discharge rate. These particles are then discharged in the next phase of flow, as can be seen with the ratios observed in Bin 4, whereby the proportion of big particles decreases with increasing adhesion.

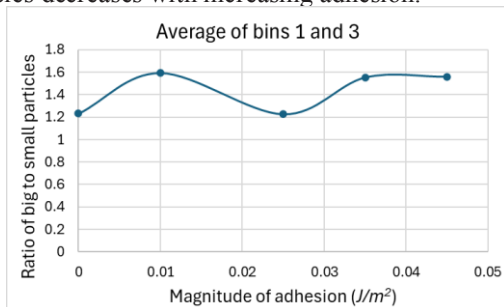


Figure 6: Ratio in bins 1 and 3 for 30° geometry

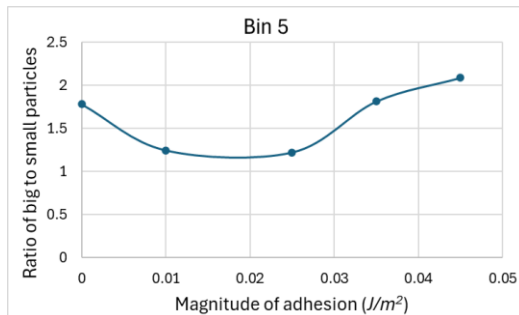


Figure 7: Ratio in bin 5 for 30° geometry

Figures 6 and 7 illustrate increasing large-to-small particle ratios with adhesion in the final phase of flow, particularly beyond  $0.025 J/m^2$ . This suggests that stronger adhesion begins to heavily influence larger particles in this phase, impeding their flow as they work against these adhesive forces. These bins then become dominated by the larger particles.

From these results, we observe that segregation is initially driven by percolation during particle loading. Adhesion to the wall primarily affects finer particles in the initial phase, while stronger adhesive forces influence larger particles higher up in the geometry.

This indicates that at lower adhesion values, finer particles dominate the segregation behaviour, whereas only stronger adhesion significantly impacts particles at higher positions within the geometry.

### 3.2 Analysis for the funnel flow (60°) geometry

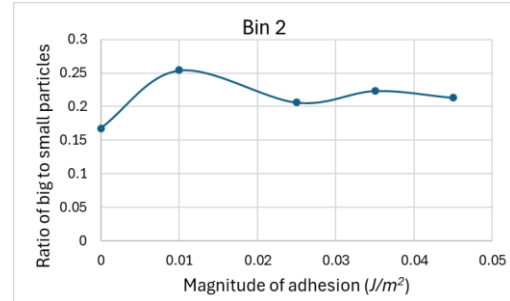


Figure 8: Ratio in bin 2 for 60° geometry

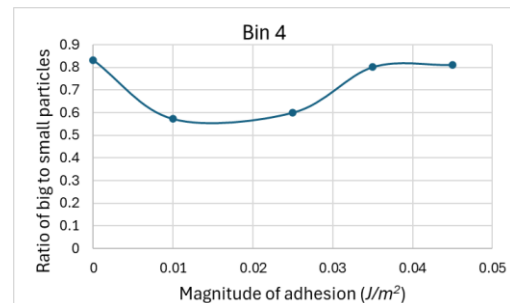


Figure 9: Ratio in bin 4 for 60° geometry

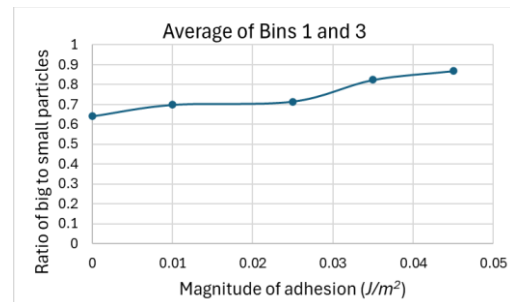


Figure 10: Ratio in bins 1 and 3 for 60° geometry

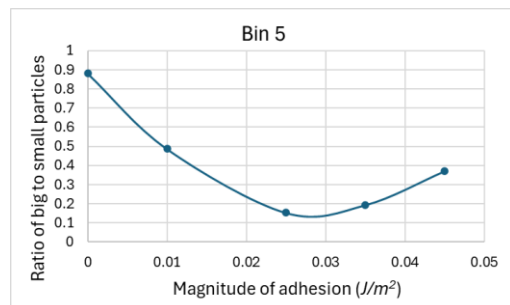


Figure 11: Ratio in bin 5 for 60° geometry

Figures 8-11 reveal that on loading, percolation-driven segregation is significant, contributing to the extremely high ratio of finer particles in bin 2 across all adhesive values. Comparing Figs. 4 and 8 shows that the percolation-driven segregation upon loading is more pronounced in the funnel flow geometry. In the 60° geometry, the ratios range from 0.15 to 0.25 for all adhesive cases, whereas in the 30° geometry, the ratios are between 0.3 and 0.4.

Figure 8 (Bin 2) demonstrates that when adhesion to the wall is introduced, finer particles are immediately affected by the pull-off force, leading to a greater proportion of larger particles moving out of the system during the initial phase. As adhesion increases from  $0.01 J/m^2$  to  $0.045 J/m^2$ , the proportion of larger particles progressively decreases. This suggests that, within the funnel flow geometry, lower adhesion magnitudes are also sufficient to influence the larger particles initially. Figure 9 (Bin 4) shows a similar trend, where the proportion of larger particles in the bulk decreases as wall adhesion is introduced, resembling the behaviour in the mass flow geometry. However, when adhesion reaches  $0.025 J/m^2$  or higher, this effect reverses, with the ratio of larger particles increasing, indicating that the flow of finer particles is significantly impacted beyond this threshold.

Figure 10 reveals that, similar to the mass flow geometry, the ratio of larger particles in Bins 1 and 3 increases as adhesive wall functions are introduced. This increase causes larger particles to exit the hopper later. Percolation leads to larger particles moving higher up the hopper, as seen in Figure 11. Initially, there is a decrease in the number of larger particles at the peak of the mound. This is likely due to smaller particles sticking to the wall higher up in the geometry, which are discharged last. When the wall adhesion exceeds  $0.025 J/m^2$ , this effect reverses, and the ratio of large particles increases with higher adhesion. This again demonstrates that lower adhesion magnitudes result in observations dominated by smaller particles, but at  $0.025 J/m^2$ , larger particles higher up in the geometry are affected.



Figure 12: Image shows the top 20% of particles based on diameter for the simulation with  $0.045 J/m^2$  of adhesion.



Figure 13: Image shows the bottom 20% of particles based on diameter for the simulation with  $0.045 J/m^2$  of adhesion.

Figures 12 and 13 show that in the funnel flow geometry with  $0.045 J/m^2$  adhesion, significant layer segregation occurs. Percolation during loading results in an increased proportion of fines in Bin 2. The layers form with heavier, larger particles at the bottom, followed by finer particles, which discharge in the next phase of flow. This is followed by a layer of the larger particles that were initially driven upwards in the hopper via percolation. Finally, the remaining fines, including those adhering to the wall, fall out. This segregation effect becomes more pronounced with higher adhesion.

## 4 Conclusions

Thus, for gravitational settling and discharge from a hopper, segregation in both mass and funnel flow geometries is induced by percolation during loading. In mass flow geometries, wall adhesion primarily affects finer particles in the lower regions, influencing their discharge during the initial flow phase. This effect, observed in bins 2 and 4, is driven by the behaviour of these fine particles. As height increases, adhesion increasingly impacts the larger particles. In funnel flow geometries, however, wall adhesion influences the flow of larger particles throughout the geometry. At higher regions, adhesive forces above  $0.025 J/m^2$  significantly hinder the movement of finer particles, reversing earlier trends. This leads to layered segregation during discharge, forming alternating bands of fine and coarse particles. Ongoing studies are investigating how wall adhesion contributes to particle clustering, the effects of bin size and filling methods, and their roles in granular segregation.

## References

- 1) S. Albaraki, S.J. Antony. 2014. Powder Technology, **264**, 253-260. <https://doi.org/10.1016/j.powtec.2014.08.027>
- 2) D.S. Shah, K.K. Moravkar, D.K. Jha, V. Lonkar, P.D. Amin, & S.S. Chalikwar, 2023. Heliyon, **9(6)**, e216498. Available from: <https://doi.org/10.1016/j.heliyon.2023.e16498>
- 3) Make UK (The Manufacturers organisation). 2023. [Online]. Accessed: 01/05/2024. <https://www.makeuk.org/insights/publications/uk-manufacturing-the-facts-2023#/>
- 4) M. Alizadeh, M. Asachi, M. Ghadiri, A. Bayly, & A. Hassanpour, 2018. Powder Technology, **339**, 789-800. <https://doi.org/10.1016/j.powtec.2018.08.028>.
- 5) H. Xiao, Y. Fan, P.B. Umbanhowar, M. Kodam, J.F. Koch, & R.M. Lueptow, 2019. Chemical Engineering Science, **193**, 188-204. <https://doi.org/10.1016/j.ces.2018.08.039>
- 6) W.R. Ketterhegen, J.S. Curtis, C.R. Wassgren, B.C. Hancock. 2008. Powder Technology, **179(3)**, 126-143. <https://doi.org/10.1016/j.powtec.2007.06.023>
- 7) P.A. Cundall, & O.D.L. Strack, 1979. Geotechnique, **29(1)**, 47-65. <https://doi.org/10.1680/geot.1979.29.1.47>
- 8) Altair EDEM. 2025. [Online]. Accessed: 20/01/2024. Available from: [https://help.altair.com/edem/topics/creator\\_tree\\_geometries/create\\_static\\_factories\\_t.htm](https://help.altair.com/edem/topics/creator_tree_geometries/create_static_factories_t.htm)
- 9) Z. Zolek-Tryznowska, E. Bednarczyk, M. Tryznowski, & T. Kobiela, 2023. Materials (Basel), **16(9)**, 3320. <https://doi.org/10.3390/ma16093320>
- 10) C.R. Woodcock, J.S. Mason. 1987. Bulk Solids Handling, 154-202. <https://doi.org/10.1007/978-94-009-2635-6>